Chapter 8

Using paramagnetic probes to study structural transitions in proteins

Belle V. and Fournel A.

*Laboratory of Bioenergetics and Protein Engineering, UMR 7281,
Institute of Microbiology of the Mediterranean,
CNRS & Aix-Marseille University, Marseille.*

8.1 - Introduction

Thanks to technical progress in structural biology, a large number of three-dimensional structures for proteins with a wide variety of functions have been determined over the last two decades. These structures provide very important information, helping us to understand how these complex macromolecules work. However, as their dynamic properties often play an essential role, this information can be insufficient. Indeed, structural flexibility is central to numerous biological processes such as enzymatic catalysis, cellular signalling and molecular recognition, as well as the assembly of complex structures. Among the techniques that have been developed to obtain information in this field, "spin labelling" combined with EPR spectroscopy, a technique known as SDSL-EPR (for *Site-Directed Spin Labelling*) has emerged as a powerful tool for the study of structural changes occurring within proteins (see appendix 4 to this volume for a description of protein structure). SDSL-EPR consists in "attaching" one or several paramagnetic probes to well-defined sites in a protein and analysing their EPR spectrum to glean information on their environment. These probes are generally stable nitroxide-type radicals with a functional group allowing its binding to a *cysteine* residue in a protein. Although the first applications of spin labelling to proteins were performed in the 1960s in pioneering work by

H. McConnell at Stanford University [Stone *et al.,* 1965; Griffith and McConnell*,* 1966], the technique has recently been the focus of a spectacular renewal of interest thanks to progress made in molecular biology tools, allowing any amino acid in a protein to be replaced by a cysteine, and to the development of pulsed EPR techniques. Given the local nature of the information provided by paramagnetic probes, the size of the biological system studied is not a limitation, and SDSL-EPR can be applied across a vast range of systems. For example, this technique has been used to obtain structural information on large membrane-bound protein complexes which cannot be studied by conventional techniques, such as X-ray diffraction crystallography or high-resolution NMR. It is also ideally suited to the study of structural changes occurring within a protein, whether induced by an external physical process, such as illumination, or by its interaction with a physiological partner (protein, ligand, substrate). This type of application, in particular as developed by W.L. Hubbell and his group at the University of California and Los Angeles (UCLA) [Altenbach *et al.,* 1989; Altenbach *et al.,* 1990], will be dealt with in this chapter.

After a review of the EPR properties of nitroxide radicals in section 8.2, we will present the different methods used to study conformational changes by SDSL in section 8.3. In sections 8.4 and 8.5, we describe the application of these methods to two very different proteins, an enzyme: human pancreatic lipase; and a protein with an intrinsically disordered domain: the measles virus nucleoprotein. Recent developments related to other applications of SDSL can be found in review articles [Fanucci and Cafiso, 2006; Klug and Feix, 2008; Klare and Steinhoff, 2009].

8.2 - EPR spectrum and mobility of nitroxide radicals

The stability, ease of synthesis, chemical properties and EPR characteristics of nitroxide radicals explain why they are used in so many applications in EPR. Thus, they appear in this volume in chapter 3 as adducts in radical traps, and in chapter 9 as "building blocks" for the development of new magnetic materials. We will briefly review the properties that make them suitable for use as *probes* in biological macromolecules. Nitroxide radicals are π radicals in which the unpaired electron is approximately equally delocalised over the nitrogen and oxygen atoms of the N–O bond. The principal values of the $\tilde{\mathbf{g}}$ matrix are very close to $g_e = 2.0023$ and they are generally ranked in the order $g_x > g_y > g_z$ where $\{x, y, z\}$ are the principle axes represented in the inset in figure 8.1. The interaction

between the single electron and the ^{14}N nucleus ($I = 1$) produces a very anisotropic hyperfine $\tilde{\mathbf{A}}$ matrix with $A_x \approx A_y \ll A_z$ [Volume 1, exercise 4.6 and appendix 3].
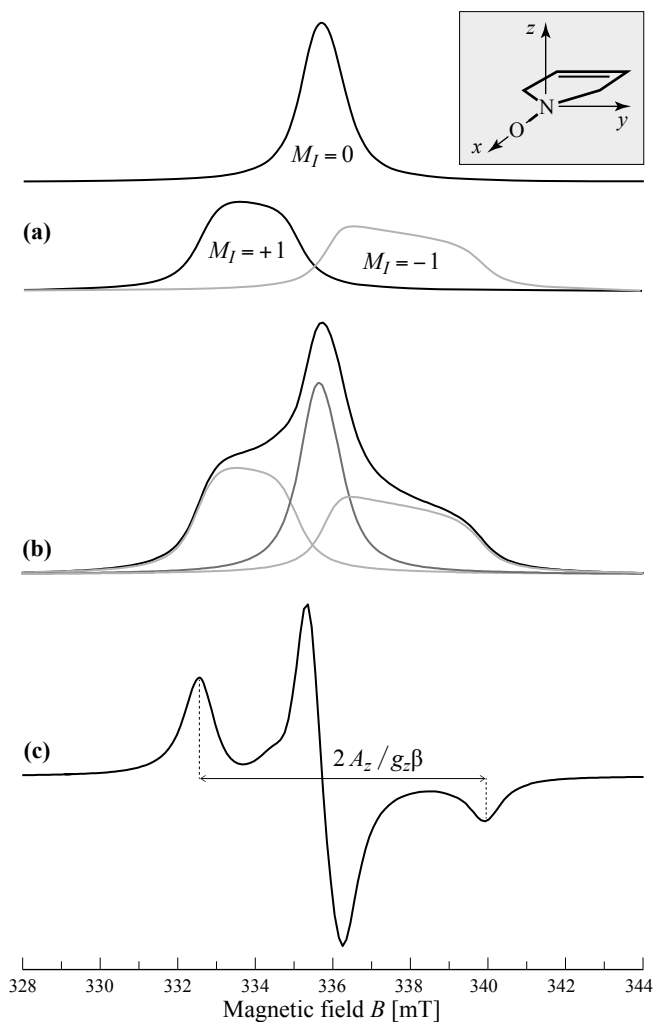

Figure 8.1 - X-band spectrum for a frozen solution of nitroxide radicals.
(a) The components corresponding to the 3 values of M_I are calculated for
$\nu = 9.428$ GHz, $(g_x, g_y, g_z) = (2.0089, 2.0064, 2.0027)$ and
$(A_x/g_x\beta, A_y/g_y\beta, A_z/g_z\beta) = (0.49, 0.49, 3.51)$ mT. **(b)** Sum of the 3 components.
(c) Derivative of the absorption signal. The (x, y, z) directions are defined in the inset.

This interaction can be considered a perturbation relative to the Zeeman term and the spectrum is the result of superposition of the three components corresponding to $M_I = -1, 0, 1$ [Volume 1, section 4.4.2]. Its shape is highly

dependent on the mobility of the molecules in the sample. The following two limit situations can be defined:

▷ In the case of a *frozen solution*, the three components are clearly separated because of the anisotropy of the hyperfine constants [Volume 1, section 4.4.3] and the spectrum spreads over a field range of around $2A_z/g_z\beta$ (figure 8.1).
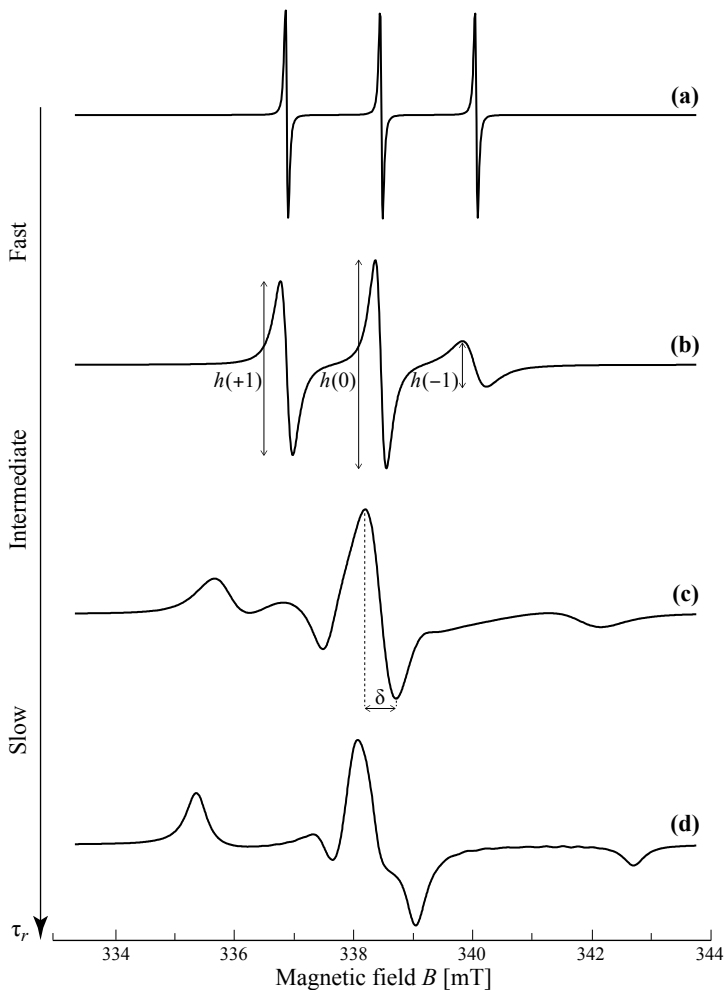
Figure 8.2 - X-band spectrum produced by a solution of nitroxide radicals undergoing isotropic movement. The spectra illustrating the different mobility regimes were calculated using *EasySpin* software [Stoll and Schweiger, 2006] for $\nu = 9.501$ GHz, $(g_x, g_y, g_z) = (2.0089, 2.0064, 2.0027)$; $(A_x/g_x\beta, A_y/g_y\beta, A_z/g_z\beta) = (0.49, 0.49, 3.51)$ mT and the following τ_r correlation times **(a)** 10^{-12} s, **(b)** 10^{-9} s, **(c)** 10^{-8} s, **(d)** 10^{-5} s. The shape of the spectrum shown in **(d)** differs from that in figure 8.1c because of its narrower linewidth. The semi-quantitative indicators used to characterise the shape of the spectrum are indicated (see section 8.3.1).

▷ In a *liquid solution*, the molecules rapidly explore all the orientations relative to the applied field with an equal probability (isotropic regime), the anisotropic effects disappear and each component reduces to a single line. The spectrum is thus a simple pattern of 3 equidistant narrow lines separated by $A_{iso}/g_{iso}\beta$, centred at $B = h\nu/g_{iso}\beta$ [Volume 1, section 2.3.3], where:

$$g_{iso} = \frac{g_x + g_y + g_z}{3} \; ; A_{iso} = \frac{A_x + A_y + A_z}{3}$$

Between these two limit situations, the calculation is more complicated, but as long as the motion of the radicals remains *isotropic*, the shape of the spectrum depends on only one parameter: the *rotational correlation time* τ_r. Some free software can calculate the EPR spectrum in this situation.

Figure 8.2 illustrates four spectral shapes calculated for four different values of τ_r:

▷ $\tau_r < 10^{-11}$ s: isotropic regime (figure 8.2a).

▷ 10^{-11} s $< \tau_r < 10^{-9}$ s: the three lines broaden without changing position (fast motion regime, figure 8.2b).

▷ 10^{-9} s $< \tau_r < 10^{-6}$ s: the spectrum broadens and spreads (intermediate regime, figure 8.2c).

▷ $\tau_r > 10^{-6}$ s: all the effects of anisotropy are observed on the spectrum (slow motion regime, figure 8.2d).

When the movement of the nitroxide radicals is not isotropic, several parameters must be used to characterise it and the spectrum is more difficult to calculate (see section 8.3.1).

8.3 - Studying structural transitions by spin labelling

Before describing the various methods used to obtain information on conformational changes occurring in proteins by SDSL, we will indicate how the labelling operation itself is performed. The nitroxide radical most frequently used to label proteins is the commercially-available compound MTSL (1-oxyl-2,2,5,5-tetramethyl-δ^3-pyrroline-3-methyl-methanethiosulfonate) which binds covalently to *cysteine* amino acid residues, forming a disulfide bridge (figure 8.3).
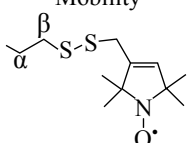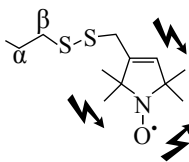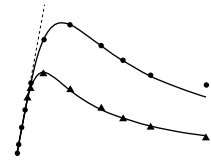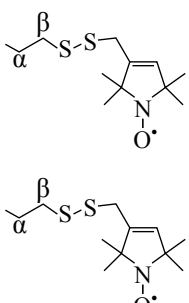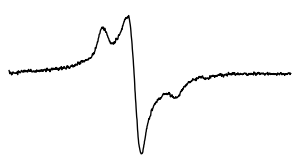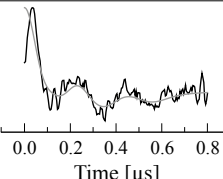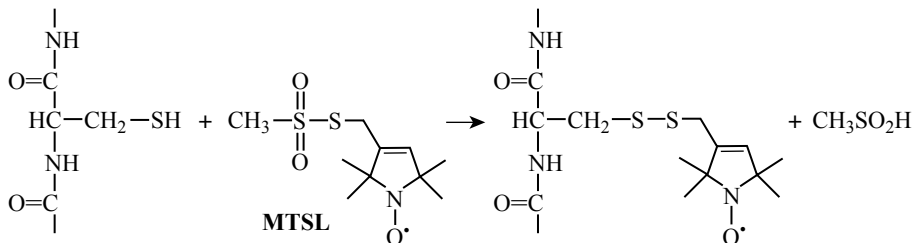
Figure 8.3 - Labelling of a cysteine with the MTSL radical.

Generally, the labelling reaction is performed by allowing the cysteine-bearing protein to react for a few hours with the label, which is present in excess. The excess unreacted label is then eliminated by gel filtration. Labelling yields obtained with this method are generally around 80 %. To label a well-defined position in the polypeptide chain, it is not sufficient to replace the amino acid located at this position by a cysteine; in addition, the cysteine residues naturally present and likely to be accessible to MTSL must be replaced by other residues. These operations are performed by "site-directed mutagenesis", i.e., by introducing appropriate modifications to the gene sequence coding for the protein (see appendix 4 to this volume). These modifications and the binding of the probe could be thought to perturb the structural changes under investigation. However, the presence of the probe generally has no, or very little, effect on the structure or function of the protein studied. This is due to the flexibility of the side chain carrying the label and the relatively low steric hindrance of the pyrrolidinyl cycle. It is nevertheless very important to verify whether the modifications affect the mutated protein, both before and after labelling (see sections 8.4 and 8.5).

In figure 8.4 we have summarised the various strategies used to obtain information on conformational changes by SDSL:

▷ The first involves analysis of *changes in mobility* for a probe bound to a region undergoing a structural transition [Steinhoff *et al.,* 1994; Thorgeirsson *et al.,* 1997; Klug *et al.,* 1998; Perozo *et al.,* 1999; Kim *et al.*, 2007; Belle *et al.*, 2008].

▷ Another, complementary, approach consists in revealing *variations in the accessibility* of the probe through the addition of relaxing agents. This technique is of particular interest for the study of membrane protein topology

[Hubbell *et al.*, 1998; Fanucci *et al.*, 2003; Altenbach *et al.*, 2005; Pyka *et al*., 2005].

Approach	Method	Signal
Mobility	Continuous wave Shape of spectrum	
Accessibility	Continuous wave Saturation Relaxing agents	
Inter-probe distance	Continuous wave Broadening Dipolar interactions	
	Pulsed EPR Double electron-electron resonance Dipolar interactions	

Figure 8.4 - Various strategies used to obtain information by SDSL.

▷ SDSL can also be used to measure *variations in the distance* between two sites in a protein. For these measurements, a label is bound to each site and the distance between the labels is determined by analysing their dipole-dipole interaction [Volume 1, section 7.2.4]. The development of pulsed EPR techniques considerably broadened the field of application of this method [Jeschke *et al.*, 2005; Altenbach *et al.*, 2008; Drescher *et al.*, 2008; Sugata *et al.*, 2009; Ranaldi *et al.*, 2010].

8.3.1 - Analysis of probe mobility

The EPR spectrum recorded at room temperature for a solution of labelled proteins is determined by the motion of the radical probes relative to the applied

magnetic field. This motion is the result of the composition of the "local" motion of the radical relative to the protein, and the rotational Brownian motion of the protein molecules in solution. When the molar mass of the proteins exceeds around 50 kDa, the protein moves much more slowly than the radical, and the proteins can be considered to be immobile and randomly oriented relative to the magnetic field. In this case, the shape of the EPR spectrum is only determined by the steric restrictions affecting the radical bound to the protein. When these restrictions are stringent, the spectrum is close to that of a frozen solution of radicals (figure 8.2d).

General rules for the qualitative interpretation of the EPR spectrum of labelled proteins were established in 1996 by Hubbell and collaborators. These authors bound a probe to various sites on T4 lysozyme, the structure of which was known, and assessed its mobility using "shape indicators" measured directly on the spectrum: width δ of the central line (figure 8.2c) and second moment of the spectrum [Hubbell *et al.*, 1996; Mchaourab *et al.*, 1996]. The results indicated that the mobility of the radical increases in the following order: buried sites, sites involving interactions with neighbouring structural elements, sites accessible to the solvent at the surface of α helices, sites located on loops at the protein's surface (see appendix 4). When probes are bound to the surface of an α helix, examination of the EPR spectra suggests that the probe's mobility is practically independent of the nature of the amino acids neighbouring the binding site, and that it is mainly determined by interaction between the S–S bond and the polypeptide chain (figure 8.3). This interpretation was confirmed by analysis of the crystal structures of the various labelled forms of T4 lysozyme [Langen *et al.*, 2000]. This study also revealed that the side chain bearing the probe can take several orientations relative to the peptide chain, with each position producing a spectral component corresponding to a structural sub-group known as a *rotamer*.

Since these first studies, the influence of fluctuations of the polypeptide chain on the EPR spectra for bound nitroxide radicals has been studied in detail [Columbus *et al.*, 2001; Columbus and Hubbell, 2002]. The consequences of the existence of several rotamers of the side chain on the shape of the spectrum have also been analysed [Guo *et al.*, 2007; Guo *et al.*, 2008; Fleissner *et al.*, 2009]. These consequences are essential to consider when using the SDSL technique to reveal conformational changes in proteins. Indeed, the spectrum produced

by a single protein conformation in which the probe can explore two different environments is identical to that which would be produced by two different conformations in which the probe explores the same environment. To distinguish between these two situations, various methods have been proposed, based on molecular dynamic calculations [Pistolesi *et al.*, 2006; Ranaldi *et al.*, 2010] or measurement of the spin-lattice relaxation time T_1 [Bridges *et al.*, 2010].

The studies mentioned above show that using indicators of the shape of the spectrum gives ready access to important information. In the *fast regime*, the best parameters to describe mobility of the radical are the ratios between the peak-to-peak amplitudes for the lateral lines labelled $h(M_I = \pm 1)$ and that of the central line $h(M_I = 0)$, which actually reflect the differences between the *widths* of the lines (figure 8.2).

▷ When the radical performs *isotropic* movement, the linewidth takes the form $\Delta B = W + a + bM_I + cM_I^2$, where W is the residual width and a, b, c are coefficients proportional to the rotational correlation time, which depends on the principal values of the $\tilde{\mathbf{g}}$ and $\tilde{\mathbf{A}}$ matrices [Goldman *et al.*, 1972] (also see Volume 1, section 5.4.1). In this case, the best indicator of the mobility of the label is the $h(-1)/h(0)$ ratio [Qu *et al.*, 1997].

▷ *Anisotropic* radical movement can be considered to result from rapid rotational movement around the y axis (inset in figure 8.1) characterised by a rotational correlation time $\tau_{//}$, and a slower rotational motion around an axis perpendicular to y, characterised by $\tau_\perp$ [Goldman *et al.*, 1972; Marsh *et al.*, 2002]. In this case, the $h(+1)/h(0)$ ratio is a better indicator of radical mobility than the $h(-1)/h(0)$ ratio [Morin *et al.*, 2006; Belle *et al.*, 2009]. We will describe an example of the use of these semi-quantitative parameters in section 8.5.1.

To interpret the EPR spectrum in a more quantitative manner, it must be simulated from an appropriate model. Several models have been proposed and we will briefly describe two. In the MOMD (*Microscopic Order Macroscopic Disorder*) model developed by J. Freed and collaborators, motion of the side chain to which the radical is bound is characterised by two parameters: an order parameter linked to *the amplitude of the motion* and an effective correlation time associated with the *rotation rate* [Freed, 1976; Budil *et al.*, 1996; Barnes *et al.*, 1999]. In another model, the rotational correlation time is considered to always be very short and the variations of the spectrum for the radical mainly reflect those of the *steric hindrance* of the movement [Stopar *et al.*, 2005;

Strancar *et al.*, 2005]. This model describes the *conformational space* explored by the probe as an asymmetric cone defined by two angles corresponding to the amplitude and the anisotropy of the movement. An example of application of this model will be given in section 8.5.2.

8.3.2 - Determining probe accessibility

The addition of a "relaxing agent" (metal complexes or O_2 molecule) to a solution of labelled proteins results in accelerated relaxation of the radicals. The acceleration is increased when the labelled site is accessible to the relaxing agent. We will see that quantitative study of this effect, based on saturation of the spectrum for the radical, can be used to assess its accessibility.

Collisions between molecules of relaxing agent and nitroxide radicals bound to the proteins create transient complexes. In these complexes, strong exchange coupling between the two paramagnetic entities produces a paramagnetic ground state, but its EPR spectrum is not observable at room temperature. When exchange between the complexed and free forms of the nitroxide is slow, the positions of the resonance lines for the radical remain unchanged, but the *lifetime* of its spin states is shortened. If k_{ex} [M^{-1} s^{-1}] is the rate constant characterising formation of these complexes, the relaxation rates for the nitroxide radical are given by the following equations [Altenbach *et al.*, 2005]:

$$1/T_1^R = 1/T_1^0 + k_{ex} C_R$$
$$1/T_2^R = 1/T_2^0 + k_{ex} C_R$$

[8.1]

where T_1^0 and T_2^0 are the relaxation times in the absence of relaxing agent, and C_R is the molar concentration of the agent. These expressions have the same form as equation [11.2] in chapter 11, which describes acceleration of the relaxation of protons from water by Gd^{3+} complexes. They indicate that the rate constant k_{ex}, which depends on the *accessibility* of the radical to the relaxing agent, can be deduced from the variation of the relaxation rates. To measure this variation, experimental saturation curves for the EPR signal of the radical are constructed, and they are simulated using an appropriate model [Volume 1, sections 5.3.2 and 9.4]. If the concentration C_R is not excessive, the variation of T_2 is negligible and the increase in power at half-saturation $P_{1/2}$ due to the relaxing agent can be written:

$$\Delta P_{1/2} = P_{1/2}^R - P_{1/2}^0 = \frac{2^{1/\varepsilon} - 1}{\frac{\gamma^2}{4} \lambda^2 T_2} \left[\frac{1}{T_1^R} - \frac{1}{T_1^0} \right]$$

[8.2]

where $P_{1/2}^0$ and $P_{1/2}^R$ are the half-saturation powers in the absence and presence of the relaxing agent, $\gamma = g\beta/\hbar$ is the magnetogyric ratio, and ε is the inhomogeneity factor for the line. ε varies from $\frac{3}{2}$ for a completely homogeneous line to $\frac{1}{2}$ for a completely inhomogeneous line [HAAS *et al.*, 1993]. λ is the "conversion factor" for the cavity defined by $B_1 = \lambda\sqrt{P}$. Its value is provided by the manufacturer or can be measured. Analysis of the linewidth in the spectrum gives T_2, and the $P_{1/2}^R$, $P_{1/2}^0$ and ε parameters can be deduced from simulations of the saturation curves in the absence and presence of a relaxing agent. Equation [8.2] can then be used to calculate the $\dfrac{1}{T_1^R} - \dfrac{1}{T_1^0}$ difference and thus deduce the rate constant k_{ex} for equation [8.1]. Sometimes a dimensionless relative accessibility Π is also used, it is defined as follows:

$$\Pi = \frac{\dfrac{\Delta P_{1/2}}{\delta}}{\left(\dfrac{\Delta P_{1/2}}{\delta}\right)_{ref}} \qquad [8.3]$$

Division by the width δ of the central line normalises the spectrum relative to T_2 (equation [8.2]), and division by the quantity $\left(\dfrac{\Delta P_{1/2}}{\delta}\right)_{ref}$, determined by studying the effect of the relaxing agent on saturation of a reference molecule such as DPPH, eliminates the λ parameter which can be difficult to determine.

To construct the saturation curves, the EPR spectrum for the nitroxide radicals must be sufficiently saturable, even in the presence of agents accelerating relaxation. This is generally impossible at room temperature when using standard cavities, and samples must therefore be analysed in specific "high conversion factor" cavities. Different relaxing agents are used depending on whether the protein studied is membrane-bound or in solution:

▷ in the case of membrane proteins, molecular O_2 is used as it tends to concentrate in membranes due to its apolar nature [Merianos *et al.*, 2000; Marsh *et al.*, 2006],

▷ in aqueous medium, Cr(III) oxalate (abbreviated as Crox) or Ni(II) ethylenediaminediacetate (abbreviated as NiEDDA) are often used [Altenbach *et al.*, 1994; Lin *et al.*, 1998; Doebber *et al.*, 2008].

When studying membrane proteins, two relaxing agents with differing polarities can be used (e.g. O_2 and NiEDDA) to produce opposing concentration gradients between the membrane phase and the aqueous phase. These gradients can be

used to calculate a Φ parameter which reflects the *depth* of the paramagnetic probe within the membrane:

$$\Phi = \ln\left[\frac{\Pi(O_2)}{\Pi(\text{NiEDDA})}\right]$$

The relative accessibilities Π are defined by equation [8.3]. The Φ parameter is *positive* when the probes are deeply embedded in the membrane where collisions with O_2 dominate, or *negative* when the probes are located close to the aqueous phase where collisions with the Ni(II) complexes dominate [Altenbach *et al.*, 1994; Kaplan *et al.*, 2000].

8.3.3 - Measuring inter-probe distances

If two radicals are bound to the same protein, the interaction between the two magnetic dipoles causes splitting of the EPR lines [Volume 1, section 7.3.1]. Quantitative study of this effect, which varies with distance according to $1/r^3$, can be used to determine their distance. In practice, the technique used must be adapted depending on the value of r.

▷ When the distance is small enough for the splitting to result in visible broadening of the spectrum ($r \lesssim 20$ Å), the EPR spectrum can be simulated using an appropriate model [Rabenstein and Sgin 1995; Steinhoff *et al.*, 1997]. This method cannot be used over very short distances ($r \lesssim 8$ Å) as in these conditions exchange interactions also contribute to splitting of the lines.

▷ When the distance is too great for the effects of the dipolar interaction to be visible on the spectrum, pulsed EPR techniques can be used to extend the range of measurement to around 80 Å. Specific pulse sequences can distinguish between the effects of dipolar interactions and other types of magnetic interactions. Currently, the most frequently used sequence is the 4-pulse DEER (*Double Electron Electron Resonance*) sequence [Pannier *et al.*, 2000; Jeschke, 2002] described in section 3 of appendix 2 to this volume. Analysis of the results is complicated by the fact that inter-centre distances are generally *distributed* in proteins, but several procedures can be used to take this phenomenon into consideration [Jeschke *et al.,* 2006].

The methods described in this section are illustrated hereafter by two studies in which a protein undergoes a conformational change as a result of interaction with its physiological partner(s).

8.4 - Activation of human pancreatic lipase

Lipases are enzymes catalysing lipid hydrolysis. In humans, Human Pancreatic Lipase (HPL) is the key enzyme in fat digestion. HPL alone is soluble in water and cannot interact with its insoluble lipid substrate: the enzyme is inactive. In the presence of a small protein, colipase, and bile salts – amphiphilic molecules which ensure the formation of lipid droplets – the enzyme can adsorb at the water-lipid interface and catalysis takes place: the enzyme is said to be *activated* [Bezzine *et al.*, 1999]. HPL activity can be determined by measuring the quantity of fatty acids released during hydrolysis of a tributyrine emulsion [Thirstrup *et al.*, 1993]. The maximum specific activity of HPL is around 12,500 U/mg (1 U produces 1 µmol of fatty acid per minute).

Several groups have sought to determine HPL's mechanism of action. Significant progress was made when the crystal structures of HPL and the HPL-colipase complex were determined. In the structure of the HPL-colipase complex, the region of the protein interacting with the lipid substrate – the *active site* – is covered by a polypeptide loop known as the *lid*. This lid is open in the structure of a HPL-colipase complex crystallised in the presence of a competitive inhibitor and amphiphilic molecules [van Tilbeurgh *et al.*, 1992; van Tilbeurgh *et al.*, 1993]. These observations led to the proposal of the following mechanism:

  ▷ when HPL is in solution, alone or in the presence of colipase, the substrate cannot access the active site, which is covered by the lid (HPL is said to be in the *closed* conformation),

  ▷ in the presence of bile salts, the presence of colipase induces a *conformational change* in the enzyme causing the lid to open (HPL is said to be in the *open* conformation).

Comparison of the two crystal structures suggested this mechanism, but no evidence has yet been obtained proving that it takes place in solution. In addition, the respective roles of colipase and bile salts in the activation process remain to be defined. We therefore undertook the study of this process *in solution* using the SDSL methods described in section 8.3.

8.4.1 - Attributing spectral features to HPL conformations

To demonstrate the conformational change of the lid in solution, a MTSL probe was bound to it, and its mobility analysed. The amino acid corresponding to

aspartic acid (code D, see table 1 in appendix 4) in position 249 of the lid was selected as the labelling site, based on information from the crystal structures indicating that this site is accessible to solvent and that it does not interact with the enzyme's core in either the open or closed conformations. As HPL has a naturally accessible cysteine (code C) in position 181, labelling at position 249 requires the construction of a *double mutant* in which D249 is replaced by a cysteine, and C181 is replaced by a tyrosine. The specific activities of the mutated HPL and the labelled mutated HPL were similar to those for native HPL, indicating that the enzyme's catalytic mechanism is affected neither by the mutations nor by the presence of the probe. To define the spectral shapes which characterise the two enzymatic conformations, we examined the effect of colipase and a bile salt (sodium taurodeoxycholate) on the shape of the EPR spectrum for the MTSL radical recorded at room temperature (figure 8.5).

When alone in solution, labelled HPL produces a "narrow" spectrum corresponding to the *fast motion* regime for the probe (see figure 8.2b), with a separation between lateral lines of 3.22 ± 0.02 mT (figure 8.5a). This spectrum is not affected by the presence of colipase (figure 8.5b). In contrast, a broad component appears when the lipase is exposed to bile salts at 4 mM – a concentration which is greater than the critical micelle concentration (CMC) (figure 8.5c). The CMC, from which bile salt molecules assemble to form micelles of sodium taurodeoxycholate is around 1 mM. By varying bile salt concentrations, a sudden increase in the proportion of the broad component was observed above the CMC [Belle *et al.*, 2007]. Upon addition of colipase, this proportion increases further, reaching 75 % (figure 8.5d). The lateral lines of the broad component determined by subtraction are separated by 6.65 ± 0.05 mT (figure 8.5e), which indicates that the probe is in the *intermediate mobility* regime (see figure 8.2c).
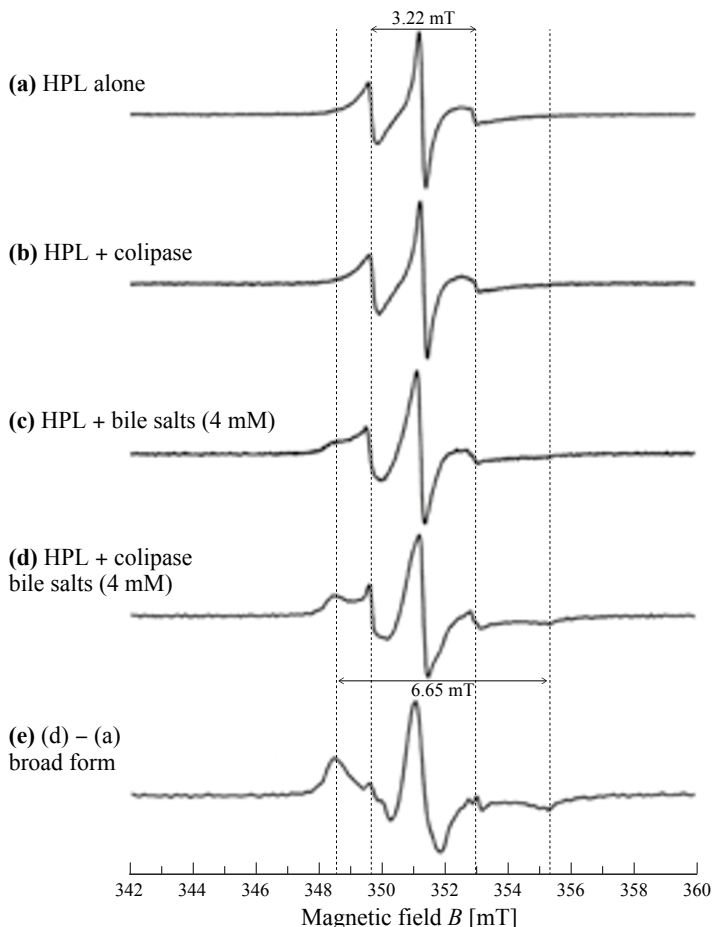
Figure 8.5 - Effect of physiological partners on the X-band spectrum for HPL labelled at position 249. **(a)** Labelled HPL in solution, **(b)** HPL in the presence of colipase (in 2-fold molar excess), **(c)** HPL in the presence of bile salts at supramicellar concentration (4 mM), **(d)** HPL in the presence of both partners, **(e)** spectrum obtained by subtraction of spectrum **(a)** from spectrum **(d)**. Microwave frequency: 9.869 GHz, power 10 mW. Modulation amplitude 0.1 mT.

Complementary experiments showed that the narrow component of the spectrum is produced by the closed conformation, and that the broad component is produced by the open conformation [Belle *et al.*, 2007] (figure 8.6). Only these two conformations were identified by SDSL. All these experiments show that colipase alone cannot induce conformational change in HPL, and that *in solution* an equilibrium between the closed and open conformations is observed

in the presence of bile salts at concentrations exceeding the CMC; the presence of colipase shifts this equilibrium to the open conformation.
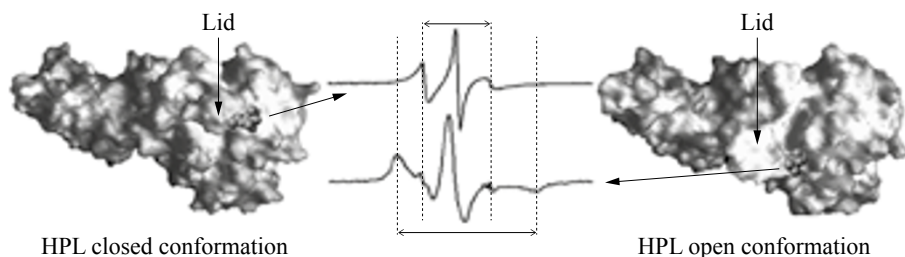
Figure 8.6 - Attributing spectral features to the two enzymatic conformations. The nitroxide radical is represented.

8.4.2 - Studying probe accessibility

The probe is less mobile when the enzyme is in the open conformation than in the closed conformation, but the reason for this difference is not obvious. To obtain some answers, we assessed *the probe's accessibility to the solvent* in these two conformations using the method described in section 8.3.2, with Cr(III) oxalate as relaxing agent. The samples studied were the following: HPL alone in solution (closed conformation), HPL in the presence of bile salts and colipase (open conformation). Saturation curves for the central line were constructed for a range of concentrations of relaxing agent, using a cavity with a high conversion factor, $\lambda = 2.0$ G W$^{-\frac{1}{2}}$ (figure 8.7). They are well reproduced by the relation

$$a_{pp} \propto \frac{\sqrt{P}}{\left[1 + (2^{1/\varepsilon} - 1)\dfrac{P}{P_{1/2}}\right]^{\varepsilon}} \qquad [8.4]$$

which describes the variation of the peak-to-peak amplitude of the derivative of an inhomogeneous line as a function of the incident microwave power, P [Haas *et al.*, 1993] (also see Volume 1, section 9.4). $P_{1/2}$ is the microwave power at half-saturation, and ε is a number describing the inhomogeneity of the line (section 8.3.2).
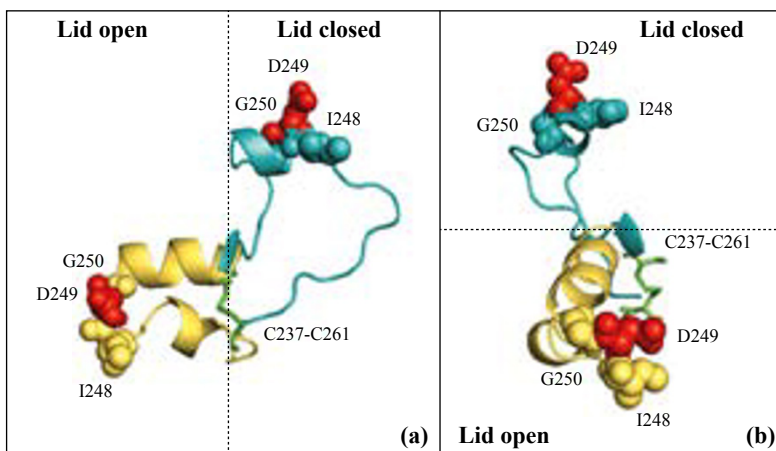
Closed conformation
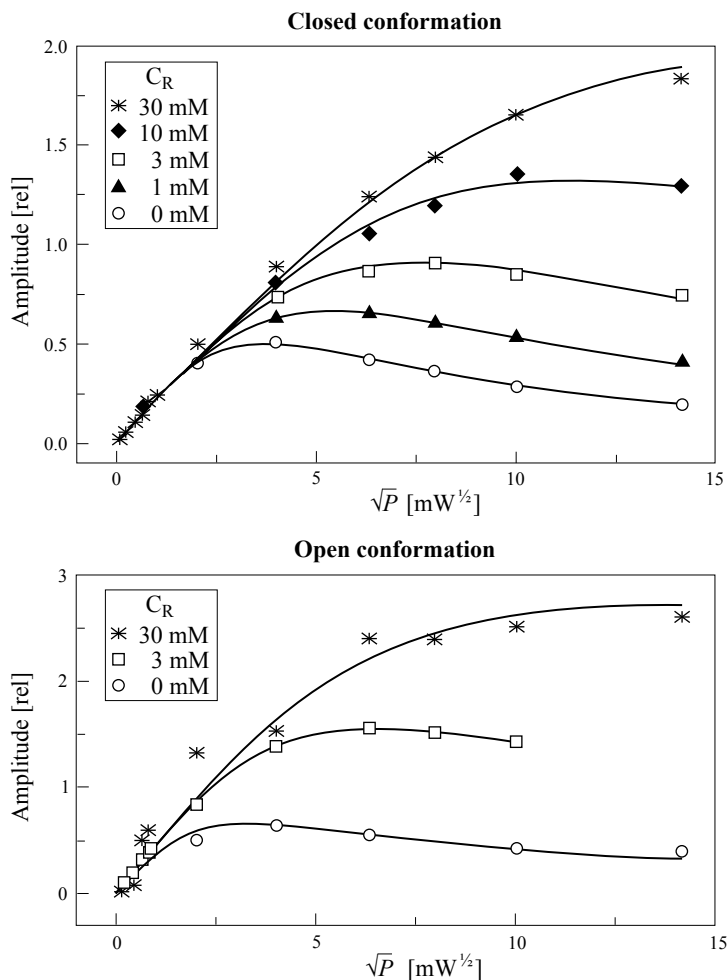
Open conformation

Figure 8.7 - Saturation curves for the MTSL radical bound to position 249 of HPL, in the closed and open conformations, for different concentrations of relaxing agent (C_R). The continuous line corresponds to calculations performed using equation [8.4].

Adjustment of the calculated curves to the experimental points returned $\varepsilon = 1.2$ for the closed conformation and $\varepsilon = 0.7$ for the open conformation. Variation of $P_{\frac{1}{2}}$ as a function of C_R can be used to determine the *exchange rate constant* k_{ex} which characterises the formation of radical-relaxing agent complexes (equations [8.1] and [8.2]). We therefore obtain:

$$k_{ex}{}^{closed} = 6.6 \times 10^8 \ \text{M}^{-1} \ \text{s}^{-1}; \ k_{ex}{}^{open} = 2.1 \times 10^8 \ \text{M}^{-1} \ \text{s}^{-1}$$

When the enzyme switches from the closed conformation to the open conformation, the exchange rate constant drops around 3-fold. The *reduced mobility* of the probe therefore correlates with a *reduction in its accessibility* to the solvent. Detailed analysis of the crystal structures suggests that aspartic acid D249 is in a less constrained environment in the closed conformation than in the open conformation (figure 8.8). It can therefore be assumed that after mutation to cysteine and binding of the probe, the latter is in a relatively free environment (probe pointing towards the solvent) in the closed conformation and a more restricted environment in the open conformation (probe trapped between two small helices). Analysis of the crystal structures could therefore help to understand the origin of the two spectral shapes observed [Ranaldi *et al.*, 2009].


Figure 8.8 - Structure of the lid showing the environment of the aspartic acid D249. Two different views **(a)** and **(b)** are shown. The C237-C261 disulfide bridge serves as a hinge for the conformational change. In the closed conformation, D249 is on a helix exposed to the solvent, whereas in the open conformation it is on a small loop trapped between two helices.

8.4.3 - Assessing the amplitude of the conformational change

To determine whether the conformational change in solution effectively corresponds to that observed on the crystal structures, the variation of the distance between two sites on the protein was estimated using the double-labelling method described in section 8.3.3. The first site, as previously, is position 249 on the lid. The second is cysteine C181, already mentioned in section 8.4.1, which is close to the active site. According to the crystal structures, the environment for this amino acid is unaltered by the conformational change (figure 8.9a). In

addition, the specific activity of the doubly-labelled HPL was similar to that of native HPL.
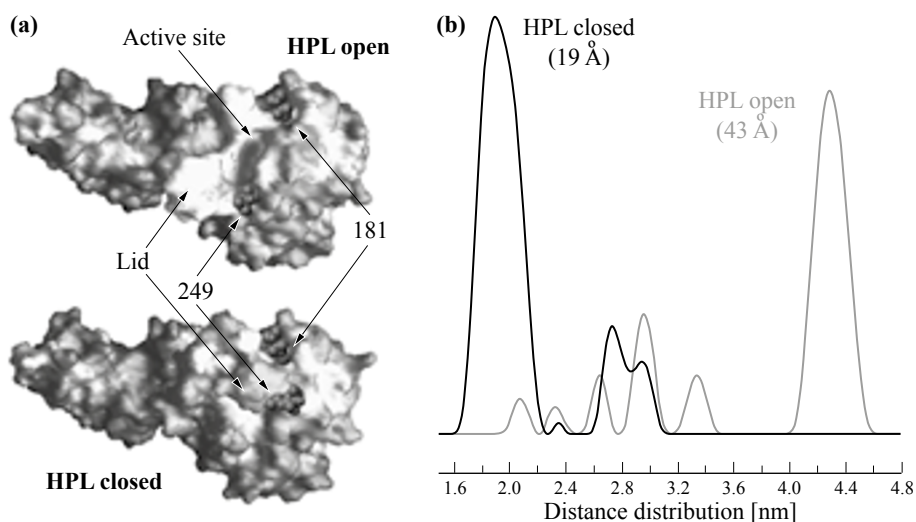
Figure 8.9 - **(a)** Modelling the positions of the two paramagnetic probes bound to positions 249 and 181 on the crystal structures of HPL in the open and closed conformations, **(b)** distribution of the inter-probe distances determined by DEER experiments performed on the closed (black line) and open (grey line) forms of the enzyme. T = 70 K, $\nu_{pump} - \nu_{obs}$ = 72.25 MHz, pulse duration 12 ns for $\pi/2$ and 24 ns for π (see section 3 in appendix 2).

DEER experiments were performed at 70 K on the HPL samples described previously, with and without the partners (colipase and bile salts at 4 mM) required to induce conformational changes. The results indicate an inter-probe distance of 19 ± 2 Å in the closed conformation and of 43 ± 2 Å in the open conformation (figure 8.9b) [Ranaldi *et al.*, 2010]. These distances are perfectly coherent with those deduced from the crystal structures, demonstrating that these structures effectively reflect the enzyme's behaviour in solution. X-band EPR spectra for the same samples were recorded at room temperature and at 100 K. Analysis of these spectra shows that for some molecules in the closed conformation, the interaction between the two radicals is visible on the EPR spectrum and it has a much larger effect than expected for a distance of 19 Å. This apparent contradiction between the results obtained by pulsed EPR and by continuous wave EPR can be explained if we remember that pulsed EPR only measures distances greater than 15 Å and if we assume that two possible orientations exist for one of the probes (two rotamers, see section 8.3.1). This

hypothesis was validated by simulation of the EPR spectra and by molecular dynamic calculations: when the probe is bound to position 249, it can take two orientations in the enzyme's closed conformation [Ranaldi *et al.*, 2010].

8.5 - Folding induced by the measles virus nucleoprotein

"Intrinsically disordered" proteins do not have a stable three-dimensional structure in physiological conditions (see appendix 4). A large number of totally or partially disordered proteins are present in living organisms, where they play essential roles in a variety of processes such as cellular regulation and cell division, molecular recognition or even processes involved in neurodegenerative diseases [Tompa, 2002; Dyson and Wright, 2005; Fink, 2005] (also see chapter 4 in this volume). The total or partial disorder of these proteins makes them highly flexible, and thus capable of interacting with multiple partners. Intrinsically disordered proteins often take a well-defined conformation when they interact with their physiological partners [Dyson and Wright, 2002; Dunker *et al.*, 2005; Uversky *et al.*, 2005]. A type of disorder-order transition, known as *induced folding*, will be dealt with in this section.

Measles remains one of the main causes of infant mortality in developing countries. According to WHO, it was responsible for 158,000 deaths worldwide in 2013. There is currently no treatment for measles, but the protein complex which allows *viral replication* is considered a prime target for the development of antiviral agents.

To better understand how this complex functions, we investigated *nucleoprotein N* – a large number of copies of which encapsidate the viral genome – and its interaction with *phosphoprotein P* – which plays an essential role in viral transcription and replication (figure 8.10). Interaction between the nucleoprotein and the phosphoprotein involves two domains: the C-terminal domain (see appendix 4) of the N protein (amino acids 401 to 525), known as N_{TAIL}, which is intrinsically disordered; and the XD domain of the phosphoprotein [Longhi *et al.*, 2003]. Study of these domains indicated that their interaction results in a part of N_{TAIL} folding into an α helix [Johansson *et al.*, 2003]. NMR, circular dichroism and small-angle X-ray diffusion experiments performed to determine the structure of the (N_{TAIL}-XD) complex only provided very partial information [Bourhis *et al.*, 2005, 2006]. We therefore undertook the study of the N_{TAIL}-XD interaction by the SDSL technique.
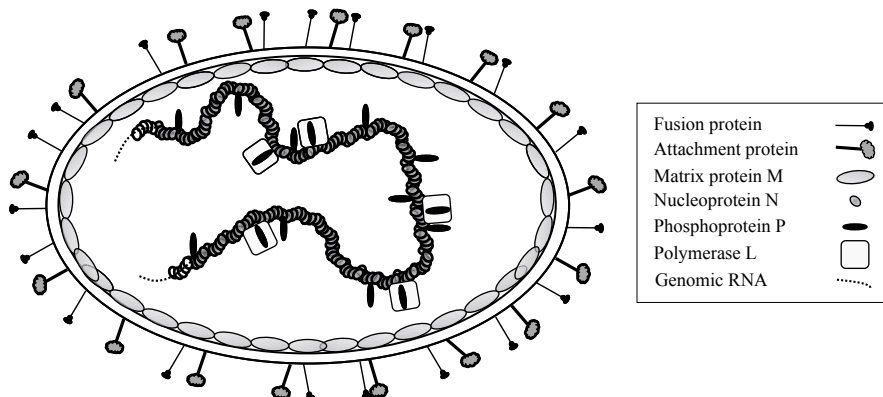
Figure 8.10 - Schematic structure of the measles virus.
Transcription and replication of the virus are ensured by the genomic RNA
and the nucleoprotein N/phosphoprotein P complexes.

8.5.1 - Mapping interaction sites for the (N_{TAIL}-XD) complex

To identify the sites on N_{TAIL} interacting with XD, we developed a series of 14 cysteine mutants of N_{TAIL} to successively probe 14 sites using MTSL. Of these 14 sites, 12 are in the 488–525 region which is known to be involved in interaction with XD, and two (positions 407 and 460) are located outside this region (top of figure 8.11). Circular dichroism experiments were used to verify that the cysteine mutations and binding of the label in the series studied affected neither the overall structure of the protein nor its folding [Belle *et al*., 2008]. The EPR spectra for the labelled N_{TAIL} domains were recorded at room temperature, alone and in the presence of XD, and the $h(+1)/h(0)$ ratio was used as an indicator of mobility of the radical (see section 8.3.1). The results are presented in figure 8.11b.

▷ As expected, the mobility of the radicals bound to positions 407 and 460 is not affected by the presence of XD.

▷ For the labels bound in the 488–502 region, the mobility indicator decreases from 0.85 to around 0.45 in the presence of XD. As an example, we have represented the spectra produced by MTSL bound to position 496 in figure 8.11a.

▷ For labels bound in the 505–522 region, the mobility indicator shifts from 0.90 to around 0.80.
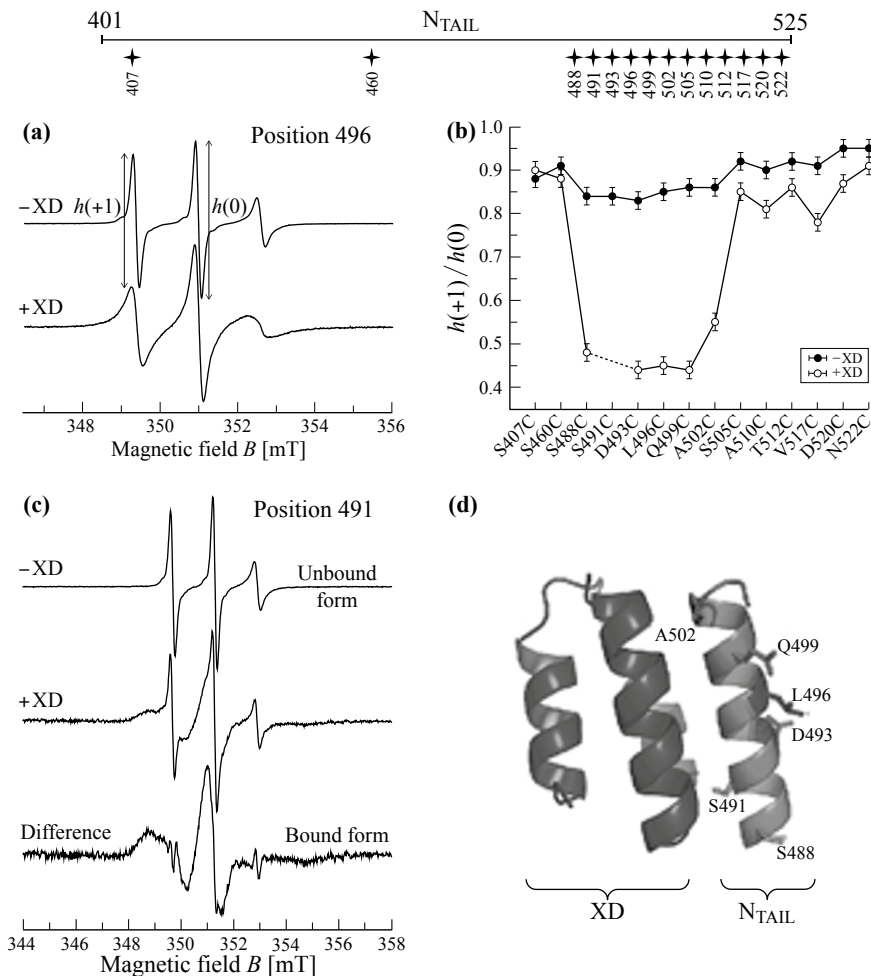
Figure 8.11 - Top: Positions of the 14 labelled sites in the 401–525 amino acid sequence of N_{TAIL}. **(a)** Spectrum for N_{TAIL} labelled at position 496, with and without XD, **(b)** variation of the $h(+1)/h(0)$ ratio as a function of the label's position, **(c)** spectrum for N_{TAIL} labelled at position 491, with and without XD. Spectra were recorded in the following conditions: microwave frequency: 9.855 GHz, power 10 mW. Modulation amplitude: 0.1 mT, **(d)** crystal structure of a chimera of XD and an N_{TAIL} region limited to amino acids 486 to 504, showing the positions of the labelled sites.

Based on these results, the N_{TAIL} region which folds as an α helix is contained between residues 488 and 502. We note that the mobility of the labels is slightly reduced in this region *before the interaction with XD*, suggesting that some *pre-structuration* exists within N_{TAIL}. This observation is compatible with a

so-called conformational selection mechanism, whereby the partner of a protein selects that with the best conformation for the interaction [Tsai *et al.*, 2001].

Labelling at position 491 produces unusual results. Indeed, the addition of XD leads to a very significant modification of the spectrum for 75 % of the proteins present, and no modification for the remaining 25 %, which therefore do not interact with XD (figure 8.11c). When the spectrum for the bound form is obtained by calculating the difference, the distance between the lateral lines is 5.95 ± 0.05 mT (figure 8.11c). This value corresponds to the intermediate mobility regime (figure 8.2c), typical of a probe located in a *buried site* [Mchaourab *et al.*, 1996]. In this complex, the probe is therefore effectively located in the region of interaction, but it is directed *towards the XD partner*.

A crystal structure for a chimeric construction resulting from the association of XD with the (486–504) region in N_{TAIL} has been obtained [Kingston *et al.*, 2004]. In this structure, the side chains of all the residues selected as binding sites are directed towards the outside of the complex, except for residue 491 which points towards XD (figure 8.11d). The results obtained by SDSL in the N_{TAIL}-XD complex therefore indicate that this structural arrangement is conserved in solution [Morin *et al.*, 2006; Belle *et al.*, 2008].

8.5.2 - Conformational analysis of the (N_{TAIL}-XD) complex

As indicated in section 8.3.1, *simulation of the EPR spectra* can provide more detailed information than that given by the mobility indicators. The model developed by Strancar and collaborators [Strancar *et al.*, 2005; Stopar *et al.*, 2006], in which rapid rotation of the probe is confined to a space restricted to a cone can be used to determine *the conformational space* of the nitroxide radical at the level of its binding site. A novel approach was developed to study the N_{TAIL}-XD complex. This approach consists in adjusting the conformational space for the probe obtained by molecular modelling, including the local conformation of the polypeptide chain described by the Ramachandran angles and the steric interactions with neighbouring residues, to reproduce the conformational space deduced from simulations of the EPR spectra. This approach confirmed the pre-structuring of an α helix in the 490–500 region in the free form of N_{TAIL}. In the presence of the XD partner, structuring as an α helix extends to the 485–506 region. Modelling also confirmed that the 507–525

region of N_{TAIL} retains a considerable degree of conformational freedom, even when bound to XD [Kavalenka *et al.*, 2010] (figure 8.12).

XD
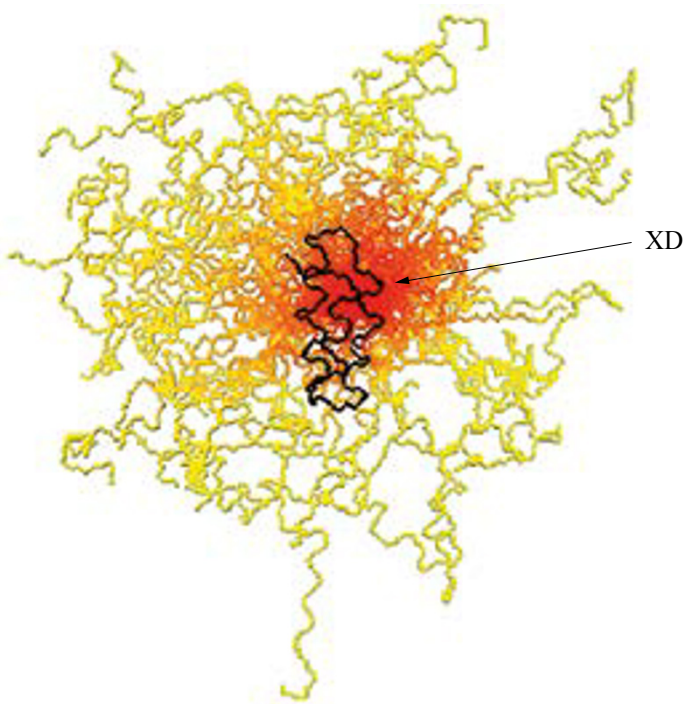
Figure 8.12 - Model of the (488–525) region of N_{TAIL} in complex with XD. The figure represents the fifty best N_{TAIL} structures obtained by adjusting the conformational space calculated by molecular modelling to that which results from simulations of the EPR spectra. The N_{TAIL} models are represented in color describing the concentrations of structures (red = high concentration, yellow = low concentration). XD is represented in black. A significant structural concentration is observed at the level of the induced helix (485–506 region) and a strong structural dispersion is observed for the upstream region (507–525 region) of the induced helix. [From Kavalenka *et al.*, 2010]

8.6 - Conclusion

In this chapter, we presented paramagnetic probe-based methods which can be used to study conformational changes occurring in proteins. These methods can be used to implement a wide range of strategies, as illustrated by their applications to two very different systems:

▷ Activation of human pancreatic lipase requires transition from the closed conformation to the open conformation, a complex phenomenon involving

several partners. Study of a probe bound *to a carefully selected site* revealed the conformational change occurring in the enzyme in solution and was used to determine the factors controlling it.

▷ We also investigated the disordered region of a viral nucleoprotein, and in particular its folding following interaction with another protein. In this case, successive labelling of a large number of sites was used to *precisely map* the region undergoing folding into an α helix. The SDSL technique had already been used to study denaturation/renaturation processes in proteins [Kreimer *et al.*, 1994; Qu *et al.*, 1997], but this is the first time that it was applied to study folding induced by another protein.

Acknowledgements

References

ALOULOU A. *et al.* (2006) *Biochimica et Biophysica Acta* **1761**: 995-1013.

ALTENBACH C. *et al.* (1989) *Biochemistry* **28**: 7806-7812.

ALTENBACH C. *et al.* (2005) *Biophysical Journal* **89**: 2103-2112.

ALTENBACH C. *et al.* (1994) *Proceeding of the National Academy of Sciences of the USA* **91**: 1667-1671.

ALTENBACH C. *et al.*(2008) *Proceeding of the National Academy of Sciences of the USA* **105**: 7439-7444.

ALTENBACH C. *et al.* (1990) *Science* **248**: 1088-1092.

BARNES J.P. *et al.* (1999) *Biophysical Journal* **76**: 3298-3306.

BELLE V. *et al.* (2007) *Biochemistry* **46**: 2205-2214.

BELLE V. *et al.* (2008) *Proteins: Structure, Function and Bioinformatics* **73**: 973-988.

BELLE V. *et al.* (2009) « Assessing Structures and Conformations of Intrinsically Disordered Proteins » in *Site-directed spin labeling EPR spectroscopy,* Uversky V.N. ed., John Wiley and Sons, New Jersey.

BEZZINE S. *et al.* (1999) *Biochemistry* **38**: 5499-5510.

BOURHIS J.M. *et al.* (2006) *Virology* **344**: 94-110.

BOURHIS J.M. *et al.* (2005) *Protein Science* **14**: 1975-1992.

BRIDGES M.D. *et al.* (2010) *Applied Magnetic Resonance* **37**: 363-390.

BUDIL D.E. *et al.* (1996) *Journal of Magnetic Resonance Series A* **120**: 155-189.

COLUMBUS L. & HUBBELL W.L. (2002) *Trends in Biochemical Sciences* **27**: 288-295.

COLUMBUS L. *et al.* (2001) *Biochemistry* **40**: 3828-3846.

DOEBBER M. *et al.* (2008) *Journal of Biological Chemistry* **283**: 28691-28701.

DRESCHER M. *et al.* (2008) *Journal of the American Chemical Society* **130**: 7796-7797.

DUNKER A.K. *et al.* (2005) *FEBS Journal* **272**: 5129-5148.

DYSON H.J. & WRIGHT P.E. (2002) *Current Opinion in Structural Biology* **12**: 54-60.

DYSON H.J. & WRIGHT P.E. (2005) *Nature Reviews Molecular Cell Biology* **6**: 197-208.

FANUCCI G.E. & CAFISO D.S. (2006) *Current Opinion in Structural Biology* **16**: 644-653.

FANUCCI G.E. *et al.* (2003) *Biochemistry* **42**: 1391-1400.

FINK A.L. (2005) *Current Opinion in Structural Biology* **15**: 35-41.

FLEISSNER M.R. *et al.* (2009) *Protein Science* **18**: 893-908.

FREED J.H. (1976) « Theory of slow tumbling ESR spectra for nitroxides » in *Spin labeling: theory and applications*, Berliner L. J., ed., Academic Press, New York.

GOLDMAN A. *et al.* (1972) *Journal of Chemical Physics* **56**: 716-735.

GRIFFITH O.H. & McCONNELL H.M. (1966) *Proceeding of the National Academy of Sciences of the USA* **55**: 8-11.

GUO Z.F. *et al.* (2008) *Protein Science* **17**: 228-239.

Guo Z.F. *et al.* (2007) *Protein Science* **16**: 1069-1086.

Haas D.A. *et al.* (1993) *Biophysical Journal* **64**: 594-604.

Hubbell W.L. *et al.* (1998) *Current Opinion in Structural Biology* **8**: 649-656.

Hubbell W.L. *et al.* (1996) *Structure* **4**: 779-783.

Jeschke G. (2002) *ChemPhysChem* **3**: 927-932.

Jeschke G. *et al.* (2005) *Journal of Biological Chemistry* **280**: 18623-18630.

Jeschke G. *et al.* (2006) *Applied Magnetic Resonance* **30**: 473-498.

Johansson K. *et al.* (2003) *Journal of Biological Chemistry* **278**: 44567-44573.

Kaplan R.S. *et al.* (2000) *Biochemistry* **39**: 9157-9163.

Karlin D. *et al.* (2002) *Virology* **302**: 420-432.

Kavalenka A. *et al.* (2010) *Biophysical Journal* **98**: 1055-1064.

Kim M. *et al.* (2007) *Proceeding of the National Academy of Sciences of the USA* **104**: 11975-11980.

Kingston R.L. *et al.* (2004) *Proceeding of the National Academy of Sciences of the USA* **101**: 8301-8306.

Klare J.P. & Steinhoff H.J. (2009) *Photosynthesis Research* **102**: 377-390.

Klug C.S. *et al.* (1998) *Biochemistry* **37**: 9016-9023.

Klug C.S. & Feix J.B. (2008) *Biophysical Tools for Biologists Vol 1 in Vitro Techniques* **84**: 617-658.

Kreimer D.I. *et al.* (1994) *Proceeding of the National Academy of Sciences of the USA* **91**: 12145-12149.

Langen R. *et al.* (2000) *Biochemistry* **39**: 8396-8405.

Lin Y. *et al.* (1998) *Science* **279**: 1925-1929.

Longhi S. *et al.* (2003) *Journal of Biological Chemistry* **278**: 18638-18648.

Marsh D. *et al.* (2006) *Biophysical Journal* **90**: 49-51.

Marsh D. *et al.* (2002) *Chemistry and Physics of Lipids* **116**: 93-114.

Mchaourab H.S. *et al.* (1996) *Biochemistry* **35**: 7692-7704.

Merianos H.J. *et al.* (2000) *Nature Structural Biology* **7**: 205-209.

Morin B. *et al.* (2006) *Journal of Physical Chemistry B* **110**: 20596-20608.

Pannier M. *et al.* (2000) *Journal of Magnetic Resonance* **142**: 331-340.

Perozo E. *et al.* (1999) *Science* **285**: 73-78.

Pistolesi S. *et al.* (2006) *Biophysical Chemistry* **123**: 49-57.

Pyka J. *et al.* (2005) *Biophysical Journal* **89**: 2059-2068.

Qu K. *et al.* (1997) *Biochemistry* **36**: 2884-2897.

Rabenstein M.D. & Sgin Y.K. (1995) *Proceeding of the National Academy of Sciences of the USA* **92**: 8239-8243.

Ranaldi S. *et al.* (2010) *Biochemistry* **49**: 2140-2149.

RANALDI S. *et al.* (2009) *Biochemistry* **48**: 630-638.

STEINHOFF H.J. *et al.* (1994) *Science* **266**: 105-107.

STEINHOFF H.J. *et al.* (1997) *Biophysical Journal* **73**: 3287-3298.

STOLL S. & SCHWEIGER A. (2006) *Journal of Magnetic Resonance* **178**: 42-55.

JONES T.J. *et al.* (1965) *Proceeding of the National Academy of Sciences of the USA* **54**: 1010-1017.

STOPAR D. *et al.* (2005) *Journal of Chemical Information and Modeling* **45**: 1621-1627.

STOPAR D. *et al.* (2006) *Biophysical Journal* **91**: 3341-3348.

STRANCAR J. *et al.* (2005) *Journal of Chemical Information and Modeling* **45**: 394-406.

SUGATA K. *et al.* (2009) *Journal of Molecular Biology* **386**: 626-636.

THIRSTRUP K. *et al.* (1993) *FEBS Letters* **327**: 79-84.

THORGEIRSSON T.E. *et al.* (1997) *Journal of Molecular Biology* **273**: 951-957.

TIMOFEEV V.P. & TSETLIN V.I. (1983) *Biophysics of Structure and Mechanisms* **10**: 93-108.

TOMPA P. (2002) *Trends in Biochemical Sciences* **27**: 527-533.

TSAI C.D. *et al.* (2001) *Critical Reviews in Biochemistry and Molecular Biology* **36**: 399-433.

UVERSKY V.N. *et al.* (2005) *Journal of Molecular Recognition* **18**: 343-384.

VAN TILBEURGH H. *et al.* (1992) *Nature* **359**: 159-162.

VAN TILBEURGH H. *et al.* (1993) *Journal of Molecular Biology* **229**: 552-554.

Volume 1: BERTRAND P. (2020) *Electron Paramagnetic Resonance Spectroscopy - Fundamentals*, Springer, Heidelberg.